

Shadow Quantum Linear Solver: A Resource Efficient Quantum Algorithm for Linear Systems of Equations

Francesco Ghisoni,^{1,*} Francesco Scala,¹ Daniele Bajoni,² and Dario Gerace¹

¹*Dipartimento di Fisica, Università degli Studi di Pavia, via Bassi 6, I-27100 Pavia, Italy*

²*Dipartimento di Ingegneria Industriale e dell'Informazione,
Università degli Studi di Pavia, via Ferrata 1, I-27100 Pavia, Italy*

(Dated: September 5, 2025)

Finding the solution to linear systems is at the heart of many applications in science and technology. Over the years a number of algorithms have been proposed to solve this problem on a digital quantum device, yet most of these are too demanding to be applied to the current noisy hardware. In this work, an original algorithmic procedure to solve the Quantum Linear System Problem (QLSP) is presented, which combines ideas from Variational Quantum Algorithms (VQA) and the framework of classical shadows. The result is the Shadow Quantum Linear Solver (SQLS), a quantum algorithm solving the QLSP avoiding the need for large controlled unitaries and requiring a number of qubits that is logarithmic in the system size. In particular, our heuristics show an exponential advantage of the SQLS in circuit execution per cost function evaluation when compared to other notorious variational approaches to solving linear systems of equations. We test the convergence of the SQLS on a number of linear systems, and results highlight how the theoretical bounds on the number of resources used by the SQLS are conservative. Finally, we apply this algorithm to a physical problem of practical relevance, by leveraging decomposition theorems from linear algebra to solve the discretized Laplace Equation in a 2D grid.

I. INTRODUCTION

The solution to a linear system of equations is at the heart of a wide range of applications in science and technology [1–4]. In its essence, the problem looks at finding $\vec{x} \in \mathbb{C}^N$ such that $A\vec{x} = \vec{b}$, where $A \in \mathbb{C}^{N \times N}$ and $\vec{b} \in \mathbb{C}^N$. The computational time for finding the solution is affected by: the system size N , the condition number of a matrix κ , the precision error ϵ , and the sparsity of the matrix.

With the first ideas dating back to the 1980's [5], the field of quantum computing aims at creating devices that change the fundamental unit of computation from a classical two level system, the bit, to a quantum two level system, the qubit [6]. This new paradigm of computation has allowed for the development of new quantum algorithms that have a computational advantage over their classical counterparts [7, 8].

In this context, of particular interest is the work by Harrow, Hassidim and Lloyd [9], who developed a quantum algorithm (also known as the HHL algorithm nowadays) to solve linear systems of equations. This can be thought as a variation of the linear system problem, in which a quantum computer is used to prepare a state $|x\rangle \propto \vec{x}$, which stores the solution. For this reason, this is also defined as the Quantum Linear System Problem (QLSP), most often. Further work following the HHL scheme [10–14] has focussed on quantum algorithms that solve a $N \times N$ sparse linear system with, among other features, a logarithmic scaling in N , which represents an exponential speed up when compared to the linear scaling of the best possible classical algorithm [9]. It is worth reminding that the exponential advantage of the HHL algorithm is at the core of the exponential advantage of many other quantum algorithms [15–19].

Despite this, the so called noisy intermediate scale quantum (NISQ) hardware available nowadays, limited both in the number of qubits and operation reliability [20], hinders the practical usefulness of any of these algorithms. In fact, the largest linear system of equations solved on quantum hardware with the HHL algorithm to date is of size $N = 8$ (i.e., corresponding to the Hilbert space size of 3 qubits) [21]. This result is due to the available hardware's inaccuracy in performing large controlled operations [22] rather than the available number of qubits, which can be in the tens [23] to hundreds [24] of qubits depending on the architecture. In the meantime, so called Variational Quantum Algorithms (VQAs) [25] have been developing as a class of hybrid classical-quantum algorithms to make use of the available NISQ hardware in the nearest terms. These algorithms run a series of parameterized quantum circuits [26], in which the parameters are iteratively updated by using classical optimization techniques. VQAs have been proposed to solve a wide range of problems, such as classification [27], chemical simulation [28–31] entanglement witness [32], solving non-linear differential equations [33, 34], and have also proposed alternatives to the HHL algorithm [35]. In particular, the Variational Quantum Linear Solver (VQLS) [36] is the most promising variational approach due to its efficient scaling in N as well as its best resource usage. As a result, the VQLS has recently become the focus of numerous applications to real-world linear systems [37–42]. Nevertheless, in most cases of practical interest this algorithm still requires large circuit depths, or large number of qubits, depending on the type of cost function to be evaluated on actual quantum hardware.

On a more general ground, the quest for optimal resource usage of quantum circuits is at the core of various protocols in quantum information [43, 44]. One such framework has been recently proposed as the *classical shadows* [45], a resource-efficient and information-complete measurement scheme that uses N_{shadow} copies of a state ρ to create the so called classical shadow $S(\rho, N_{\text{shadow}})$ of that state. Among other applications,

* francesco.ghisoni01@universitadipavia.it

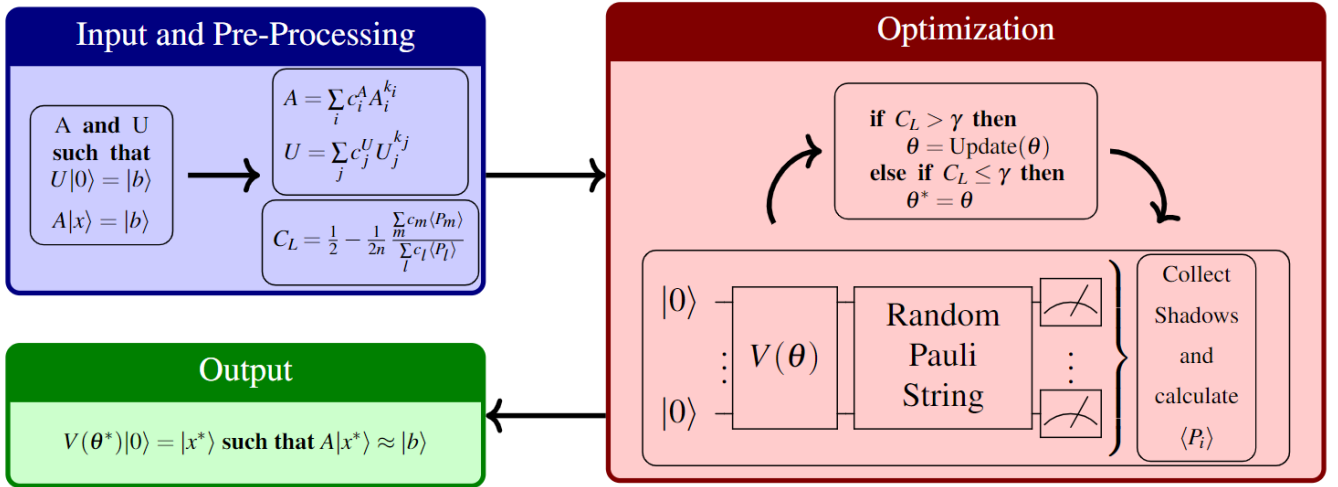


FIG. 1: Schematic diagram for the SQLS. The aim is to solve a linear system $A\vec{x}_0 = \vec{b}$. The inputs are: a matrix A , a unitary U , both written as a linear combination of Pauli strings, and form a linear system of Equations, $A|x\rangle = |b\rangle$ in which $U|0\rangle = |b\rangle$. The solution is found by using a hybrid classical-quantum variational algorithm were the parameters $\vec{\theta}$ of a parameterized quantum circuit, $V(\vec{\theta})$, will be optimized through classical optimization techniques. Due to the assumptions on the form of A and U , the cost function involves the calculation of linear sums of expectation values of Pauli strings, which can be calculated using a small number of shallow circuits through classical shadows. The optimization process terminates when the condition γ (see Eq. (14)), is reached, returning a set of parameters θ^* such that $V(\theta^*)|0\rangle = |x^*\rangle \approx \vec{x}_0$.

the shadow can be used to accurately estimate linear functions, in particular. Due to their flexibility, classical shadows have been employed in combination with VQAs for a wide range of applications, such as warm starting [46], optimizing circuits [47], and to avoid barren plateaus [48].

In this work, essentially we merge ideas from VQAs and classical shadows to present a novel procedure to solve the QLSP. Our original procedure, which we define as the Shadow Quantum Linear Solver (SQLS), leverages classical shadows to efficiently evaluate the cost function encoding the solution to a QLSP. When compared to other variational approaches to the QLSP, we notice that the SQLS uses less qubits, less controlled operations, and shallower circuits. Furthermore, in the noiseless hardware limit the SQLS offers an efficient scaling with the systems size, N , allowing to address problems that might be difficult to be solved by only using classical computing resources.

The present manuscript is organized as follows: in Sec. II we review the basics of Variational Quantum Algorithms (VQAs) and the classical shadows formalism, for completeness. In Sec. III we introduce the SQLS, showing the theoretical advantages expected in the solution of the QLSP. In Sec. IV we present the studies carried out in this work to characterize the SQLS: First, we theoretically show that SQLS is less resource intensive for more complex systems of equations when compared to other variational approaches to the QLSP; finally, we leverage techniques from linear algebra to find the solution to a real physics problem, the discretized Laplace Equation on a grid. Ultimately, we believe that the procedure hereby introduced has the potential to speed up the advent of near-term solutions of the QLSP on NISQ devices. In addition, the paper brings to attention further techniques

to transform highly non-trivial linear systems into a QLSP, which could inspire new applications of quantum algorithms to solve linear systems of equations.

II. THEORETICAL BACKGROUND

Here we report the theoretical background required to formalize the Shadow Quantum Linear Solver (SQLS). In particular, we first summarize Variational Quantum Algorithms (VQAs), and then outline the main aspects of classical shadows. Throughout the manuscript, we will adopt the convention to express Pauli gates as σ^i , in which $i \in \{I, X, Y, Z\}$, and k -local Pauli strings as $P^k = \bigotimes_{j=1}^n \sigma^j$, in which k indicates the number of non-identity elements in the string, and n is the number of qubits. Furthermore, we note that in the whole manuscript we use the shorthand notation $\log_2(\cdot) \equiv \log(\cdot)$.

A. Variational Quantum Algorithms

VQAs are a class of hybrid quantum-classical algorithms aimed at distributing the computation between a digital quantum device and a classical computer, making them ideal for the currently available NISQ devices [25]. These algorithms require the definition of a cost function C (often also called the *loss* function) whose minimum represents the optimal solution of the problem. Following this, a generic parameterized quantum circuit [26] is proposed. This circuit, also known as the *ansatz*, can be expressed as:

$$V(\theta) = G_{k_L}(\theta_L)G_{k_{L-1}}(\theta_{L-1})\dots G_{k_1}(\theta_1), \quad (1)$$

in which the quantum gates G are chosen from an alphabet $\mathcal{A} = \{G_k(\theta_i)\}$, where \vec{k} dictates the type and order of the gates and θ_i are continuous parameters. Since the cost function is defined in terms of the anstaz, it is dependent on these parameters as well, i.e. $C(\vec{\theta})$. The goal is then to find the optimal set of parameters $\vec{\theta}^*$ by minimizing the cost function,

$$\vec{\theta}^* = \arg \min_{\vec{\theta}} \{C(\vec{\theta})\}. \quad (2)$$

In the setting of Equation (2), $\vec{\theta}^*$ can be found by using classical optimization techniques. Despite this simple formulation, VQAs may suffer from flat optimization landscapes, known as *barren plateaus*, which renders both gradient based and gradient free optimization techniques poorly converging [49]. This phenomenon has been studied in depth in the literature, and various causes and possible solutions have been identified [50]. Among these, we point out two potential solutions: the first calls for the use of a *local* cost function, in which the quantum circuits undergo only single-qubit measurements [51], while the second suggests the initialization of the parameters to small values [52–54].

A further feature that some VQAs have shown to exhibit is Optimal Parameter Resilience (OPR) [55]. OPR refers to the phenomenon where the optimal parameters are not affected by a particular type of noise. In particular let \tilde{C}_L be the noisy cost function of a VQA, then OPR guarantees that $\min \tilde{C}_L = \min C_L$. VQAs which are resilient to a large number of noise models are considered especially well suited for NISQ devices.

B. Classical Shadows

Classical shadows have been formulated as a protocol allowing to construct a minimal representation $S(\rho; N_{\text{shadow}})$ of a quantum state ρ to be employed to accurately estimate functions, both linear and nonlinear, with a given error ϵ_{shadow} . When applying the procedure, we assume to have access to a fixed but unknown n -qubit quantum state ρ . The protocol is then applied by starting with a unitary U randomly chosen from a fixed ensemble \mathcal{U} , and then measured in the computational basis. The outcome, $|\alpha\rangle \in \{|0\rangle, |1\rangle\}^{\otimes n}$, is used to calculate and store an approximation of ρ , i.e.,

$$\hat{\rho} = \mathcal{M}^{-1}(U^\dagger |\alpha\rangle\langle\alpha| U), \quad (3)$$

where \mathcal{M} is a quantum channel defined as

$$\mathcal{M}(\hat{\rho}) = \mathbb{E}[U^\dagger |\alpha\rangle\langle\alpha| U]. \quad (4)$$

If the set of unitaries \mathcal{U} is tomographically complete, i.e., for each $\sigma \neq \rho$ there exists $U \in \mathcal{U}$ and b such that $\langle b|U\sigma U^\dagger|b\rangle \neq \langle b|U\rho U^\dagger|b\rangle$, then it has been shown that \mathcal{M} can be always inverted [45]. Repeating this procedure N_{shadow} times, and saving each result $\hat{\rho}_i$ in a matrix, finally produces the *classical shadow*, or shadow, $S(\rho; N_{\text{shadow}})$ defined as:

$$S(\rho; N_{\text{shadow}}) = \{\hat{\rho}_1, \hat{\rho}_2, \dots, \hat{\rho}_{N_{\text{shadow}}}\}. \quad (5)$$

This shadow can be used to estimate a wide variety of quantities, but for the purpose of the SQLS that we are going to describe in the following, we only present the algorithm and the theoretical guarantees to use $S(\rho; N_{\text{shadow}})$ to calculate M expectation values $\{\langle P_i^{k_i} \rangle\}$, where $P_i^{k_i}$ are k_i -local Pauli strings. In this case, the quantity $\langle P_i^{k_i} \rangle$ is estimated by computing :

$$\langle P_i^{k_i} \rangle = \text{median} \left\{ \text{Tr} \left(P_i^{k_i} \hat{\rho}_1 \right), \text{Tr} \left(P_i^{k_i} \hat{\rho}_2 \right), \dots, \text{Tr} \left(P_i^{k_i} \hat{\rho}_{N_{\text{shadow}}} \right) \right\}, \quad (6)$$

in which N_{shadow} depends on the error ϵ_{shadow} , and scales as

$$N_{\text{shadow}} \propto \frac{\log(M)3^k}{\epsilon_{\text{shadow}}^2}. \quad (7)$$

Furthermore we note that the same amount of shadows can be used to compute the density matrix ρ with a error $\epsilon_{\text{shadows}}$ by computing:

$$\rho = \mathbb{E}(S(\rho; N_{\text{shadow}})). \quad (8)$$

III. SHADOW QUANTUM LINEAR SOLVER

Inspired by the variational approaches to the QLSP, we hereby present the Shadow Quantum Linear Solver (SQLS), a new resource efficient VQA aimed at leveraging the power of classical shadows in the context of solving linear systems of equations. Our proposal claims efficient resource utilization as well as, in the noiseless limit, an efficient scaling with the system size. A schematic diagram of the proposed algorithm is represented in Fig. 1.

Considering a $N \times N$ QLSP of the form $A|x_0\rangle = |b\rangle$, the SQLS aims at finding a set of optimal parameters $\vec{\theta}^*$ that, when used in a quantum circuit V , they allow to prepare the solution to the QLSP, i.e., $V(\vec{\theta}^*)|0\rangle = |x(\vec{\theta}^*)\rangle = |x^*\rangle \approx |x_0\rangle$. Hence, the SQLS requires $n = \log(N)$ qubits and two inputs: 1) a unitary U that satisfies: $U|0\rangle = |b\rangle$ and, 2) a decomposition of the matrices A and U into a linear combination of k -local Pauli strings P^k , i.e.,

$$A = \sum_{i=1}^{L_A} c_i^A A_i^{k_i} \quad (9)$$

$$U = \sum_{j=1}^{L_U} c_j^U U_j^{k_j}, \quad (10)$$

in which $c_i^A, c_j^U \in \mathbb{C}$, and $A_i^{k_i}$ and $U_j^{k_j}$ are k_i -local and k_j -local Pauli strings, respectively. Furthermore, we note that this form of U is equivalent to assuming that the operator is given in an efficient gate sequence, whilst the form of A is typical of VQAs [56]. Finally, we assume that: (1) the condition number of the matrix A is finite, $\kappa_A < \infty$, (2) the l_2 norm of A is bound by 1, $\|A\|_2 \leq 1$, (3) L_A and L_U are polynomial in n , and (4) the Pauli matrices $A_i^{k_i}$ and $U_j^{k_j}$ have a low locality. This last assumption can be seen as considering a *sparse* linear system, which is common in QLSP algorithms [9]. Furthermore,

in this regime there exist algorithms [57–61] that efficiently decompose a sparse unitary as a linear sum of Pauli strings.

With these inputs, the SQLS runs an optimization process using a local cost function analogue to the one proposed in Ref. [36]. In particular, given the un-normalized quantum state $|\psi(\vec{\theta})\rangle = A|x(\vec{\theta})\rangle$, the local cost function is defined as:

$$C_L(\vec{\theta}) = \frac{\langle x(\vec{\theta}) | H_L | x(\vec{\theta}) \rangle}{\langle \psi(\vec{\theta}) | \psi(\vec{\theta}) \rangle} = \frac{\langle x | H_L | x \rangle}{\langle \psi | \psi \rangle}, \quad (11)$$

in which we employ the compact notation $|x(\vec{\theta})\rangle = |x\rangle$, and the effective Hamiltonian is explicitly expressed as:

$$H_L = A^\dagger U \left(\mathbb{I} - \frac{1}{n} \sum_{j=1}^n |0_j\rangle\langle 0_j| \otimes \mathbb{I}_{j-} \right) U^\dagger A. \quad (12)$$

Here, \mathbb{I} is the identity matrix, $|0_j\rangle$ is the j -th qubit zero logical state, and \mathbb{I}_{j-} is the identity on all qubits except for the j -th one. The cost function in Eq. 11 effectively encodes the solution to the problem: if $C_L \rightarrow 0$, then $|\psi\rangle \rightarrow |b\rangle$, meaning that a minimization of C_L guarantees a solution to the QLSP. We now introduce the approximation error ε as:

$$\varepsilon = \frac{1}{2} \text{Tr} (|x_0\rangle\langle x_0| - |x^*\rangle\langle x^*|), \quad (13)$$

which is the trace distance between the real solution, $|x_0\rangle$, and the approximate optimal solution, $|x^*\rangle$. Then, considering a target approximation error ε , for a QLSP with the condition number κ and requiring a number of qubits n , the local cost function from Eq. (11) is bound by

$$C_L \geq \frac{1}{n} \frac{\varepsilon^2}{\kappa^2} = \gamma \quad (14)$$

in which γ is the termination threshold for the optimization process [36]. Furthermore, it has been shown that for a $N \times N$ QLSP with condition number κ , and accepting a final error ε , the noiseless cost function scales as follows [36]: poly logarithmically in the problem size N , linearly in κ , and logarithmically in $1/\varepsilon$. It is important to notice that the system size scaling guarantees an exponential advantage of the noiseless SQLS over the best classical algorithm [9]. Furthermore, it has been proposed that estimating the noiseless cost function to a $1/\text{poly}(n)$ precision belongs to the *Deterministic Quantum Computing with 1 clean qubit* (**DQC1**) complexity class. The latter contains all problems that can be efficiently solved with bounded error in the one-clean-qubit model of computation [62], which has been suggested to be impossible to simulate on a classical computer [63, 64].

Given the setting of the linear system introduced in Eqs. (9) and (10), the cost function can be re-written in a compact notation as

$$C_L = \frac{1}{2} - \frac{1}{2n} \frac{\mu}{\omega}, \quad (15)$$

in which

$$\mu = \sum_{r=1}^n \sum_{i,j=1}^{L_A} \sum_{l,p=1}^{L_U} c_i^A c_j^{A*} c_p^U c_l^{U*} \delta_{ijlp}^k \quad (16)$$

$$\omega = \sum_{i,j=1}^{L_A} c_i^A c_j^{A*} \beta_{ij}, \quad (17)$$

with $\delta_{ijlp}^r = \langle x | A_j^{k_j\dagger} U_p^{k_p} \sigma_r^z U_l^{k_l\dagger} A_i^{k_i} | x \rangle$ and $\beta_{ij} = \langle x | A_j^{k_j\dagger} A_i^{k_i} | x \rangle$. Here, σ_r^z represents a σ^z on the r -th qubit. At this stage, it is important to point out that μ and ω are, essentially, weighted sums of expectation values of Pauli strings. Since the evaluation of the cost function requires the estimation of many expectation values of Pauli strings, one can leverage classical shadows, and in particular Eq. (6), to efficiently perform this operation. More in detail, given $|x\rangle$ with associated density matrix ρ_x , we define its classical shadow as $S(\rho_x, N_{\text{shadow}})$, where N_{shadow} is determined following Eq. (7). Due to the very efficient resource use of classical shadows, the advantage of using the SQLS is two-fold: circuits are shallow, and N_{shadow} scales logarithmically with the number of expectation values to calculate. A full investigation of the resources required in a SQLS run is given in Sec. IV A.

Once the optimization process is over, Eq. (8) can also be used to reconstruct the density matrix of the state $|x^*\rangle \approx |x_0\rangle$ without any additional measurement, since classical shadows also allow for quantum state tomography [45]. This is a non-trivial addition to have as part of the algorithm, since the state vector reconstruction requires, in general, an exponential amount of measurements to the circuit [65]. For example, both in the HHL and the VQLS the solution to the linear system can only be extracted through tomographic procedures, which would cancel out the exponential advantage offered by running both algorithms. Therefore, eliminating the need for a final tomography of the output quantum state the SQLS significantly reduces both the amount of resources required as well as the computational time.

Finally, we address the Optimal Parameter Resilience(OPR) of the SQLS. In fact, in [36] it was proven that the cost function of the form of Equation (11), when evaluated with the hadamard test, exhibits OPR to both a global depolarizing channel as well as measurement noise. We argue that the OPR to a global depolarizing channel is inherited in the SQLS whilst, due to the fact that shadow collection requires multiple qubit measurements, OPR to measurement noise is not inherited. The qualitative arguments for OPR in the SQLS can be found in App. A.

To summarize the SQLS algorithm, where the main steps are reported in Fig. 1, given the inputs of Eqs. (9) and (10). First, we define a parametrized ansatz V , and initialize it with a set of parameters $\vec{\theta}$. This is followed by the optimization process, which involves the creation of the classical shadow of the ansatz state $V(\vec{\theta})|0\rangle$, followed by the calculation of the local cost function C_L as defined in Eq. (15), and the update of parameters through classical optimization techniques. This optimization step is repeated until the termination threshold γ (defined in Eq. (14)) is met by C_L . This will terminate the optimization process and the SQLS will give the state $|x^*\rangle$ as

its output, i.e., the state in which the solution to the QLSP is encoded.

IV. RESULTS

We now report a number of theoretical studies aimed at granting an analytic and heuristic understanding of the SQLS. Section IV A is devoted to understanding the resource usage of the SQLS, and comparing it to the VQLS [36], which is the currently most resource-efficient variational approach to the QLSP, to our knowledge. Then, in Sec. IV B we study the heuristics of the convergence times of the SQLS for a number of different linear systems. Finally, in Sec. IV C we are able to leverage techniques from linear algebra to apply the SQLS to a real physics problem, the discretized Laplace equation in a 2D grid, and find its solution. In the following, all quantum circuits are simulated using the python Pennylane library [66].

A. Resource investigation

The first heuristic study carried out on the SQLS looks at quantifying the resource used in performing the evaluation of the cost function defined in Eq. (15). Within the investigation, we consider three variables: number of qubits, circuit depth and number of circuits per cost function evaluation. We start with the comparison between the SQLS and the VQLS, by analysing the requirements in terms of circuit depth and number of qubits to evaluate a single term in the cost function. We will assume that both algorithms have the same $n = \log N$ qubit ansatz $V(\vec{\theta})$. The assumptions made on the linear system are the same as in Sec. III, i.e. the linear system can be expressed as in Eqs. (9) and (10), and the cost function is given in Eq. (15).

For the SQLS, the scaling of both the circuit depth and the number of qubits is solely determined by the ansatz $V(\vec{\theta})$. In fact, as described in Sec. III, at each iteration the SQLS creates a classical shadow $S(\rho_x, N_{\text{shadow}})$ that is then used to approximate all the required expectation values in Eq. (15). The creation of the shadow is done by applying $V(\theta)$ to $|0\rangle^{\otimes n}$, followed by the application of a random Pauli string with a locality based on the terms in Eqs. (9) and (10), before performing a measurement over the whole register. Since no additional ancillary qubit is required, $n_{\text{SQLS}} = \log N$. Furthermore, since the application of a Pauli string has depth 1, the scaling of the circuit depth is determined by the depth of the ansatz $V(\vec{\theta})$ plus a constant. The circuit implementation of the SQLS can be schematically seen in Fig. 2a(i).

For the VQLS, instead, the scaling of the circuit depth is determined by the ansatz as well as the locality of the terms in Eqs. (9) and (10); in this case, the minimal number of qubits required is $n_{\text{VQLS}} = \log N + 1$. This is because the VQLS uses the Hadamard test to estimate the expectation values, a procedure that exploits an extra ancillary qubit (i.e., the $+1$ in the expression above). In addition, the Hadamard test requires large controlled operations to calculate the terms δ_{ijl}^r

(Eq. (16)) and β_{ij} (Eq. (17)). The circuit implementation to calculate β_{ij} and δ_{ijl}^r can be schematically seen in Figs. 2a(ii) and 2a(iii), respectively. Full details on the Hadamard test to calculate β_{ij} and δ_{ijl}^r are given in App. B, for completeness. Therefore, the SQLS uses 1 less qubit and, most importantly, removes the need for large controlled unitaries outside the ansatz $V(\vec{\theta})$, which typically require a large number of two-qubit gates. We further notice that a classical and computationally cheap pre-processing can be performed to reduce both the locality and the total number of terms to calculate, as described in App. D. On the one hand, this would allow for a reduction in the circuit depth of the VQLS, on the other hand it would guarantee a locality reduction of the terms, thus reducing the number of shadows required by Eq. (7). Nevertheless, the Hadamard test would still require large controlled operations, meaning that the SQLS would still be advantageous both in terms of the number of qubits and circuit depth.

The third point of comparison is the number of circuits required to take an optimization step, which we denote as $N_{\text{circuits}}/\text{step}$. To simplify the analysis, we assume the linear system to be described by the following matrices

$$A = \sum_{i=1}^L c_i A_i^k \quad (18)$$

$$U = H^{\otimes n},$$

in which $c_i \in [-1, 1]$ and A_i^k are k -local Pauli strings. This form of linear system allows to characterize $N_{\text{circuits}}/\text{step}$ as a function of a single parameter, L , indicating the number of Pauli strings in the system, rather than having two parameters as in Eqs. (9) and (10) (L_A and L_U). Furthermore, having all Pauli strings with fixed locality allows to investigate the effects of the locality on $N_{\text{circuits}}/\text{step}$. Within the VQLS framework, the number of circuits (each evaluated with a precision $\epsilon_{\text{hadamard}} = 1/\sqrt{n_{\text{shots}}}$) required to evaluate the cost function of Eq. (15) for a linear system expressed as in Eq. (18) is given by:

$$\left(\frac{N_{\text{circuits}}}{\text{step}} \right)_{\text{VQLS}} = \frac{n_{\text{shots}}}{2} (L(L-1) + nL^2), \quad (19)$$

where we assume that all circuits are executed for the same number of shots, n_{shots} . Details on the derivation of Eq. (19) can be found in App. C.

Within the SQLS, instead, $N_{\text{circuits}}/\text{step}$ is given by Eq. (7). Using the same considerations as above for the VQLS, the number of circuits per step is given by:

$$\left(\frac{N_{\text{circuits}}}{\text{step}} \right)_{\text{SQLS}} = \frac{\log((L(L-1) + nL^2))3^{2k+1}}{\epsilon_{\text{shadow}}^2}. \quad (20)$$

Here, the constant of proportionality in Eq. (7) is set to 1, which our numerical experiments reported in Sec. IV B show to be a conservative value. The power of $2k+1$ is a worst-case scenario consideration for the terms δ_{ij}^r .

From a direct comparison of the equations above, we can see that the SQLS has an exponentially better scaling of the $N_{\text{circuits}}/\text{step}$ with respect to the number of terms in the linear

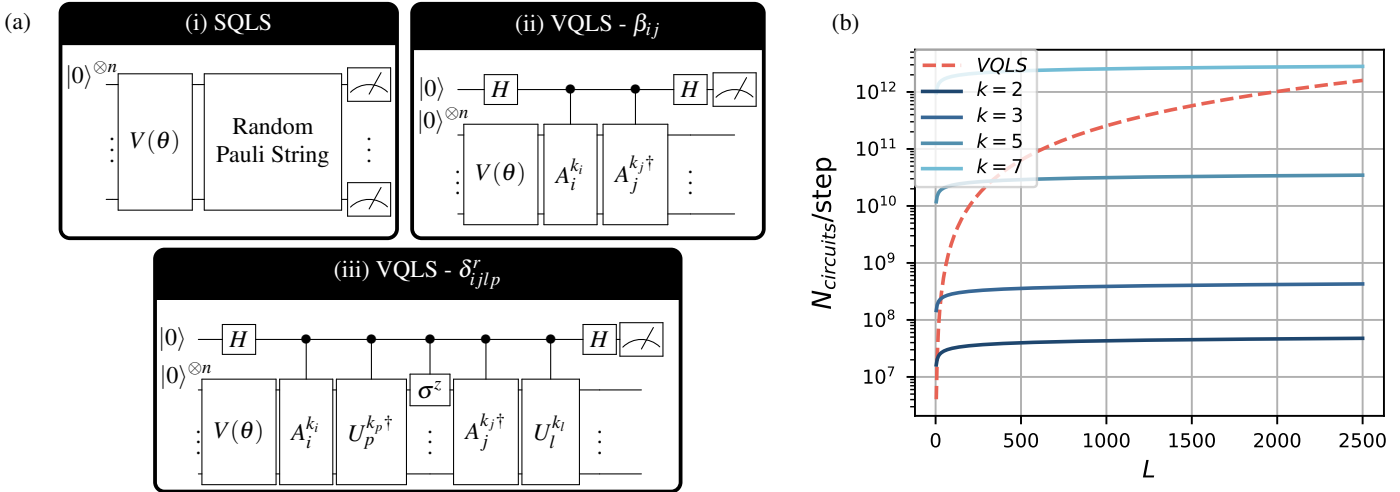


FIG. 2: The SQLS is compared to the VQLS in terms of resource usage. Panel (a) shows the schemes for the different circuit architectures employed by the two algorithms in evaluating a single term in the cost function (i.e., Eq. (15)) where: (a)(i) is the schematic quantum circuit for the SQLS, (a)(ii) and (a)(iii) are the schematic circuit implementations for the VQLS. Panel (b) shows the scaling of the number of circuits per optimization step (or evaluation of the cost function), $N_{circuits}/step$, comparing between the VQLS and SQLS, respectively. The estimate is provided for a $2^{50} \times 2^{50}$ linear system of the form given in Eq. (18), in which k indicates the locality of the Pauli strings forming the linear system. Evidently, as the number of terms in the linear system L increases (i.e., when the linear system becomes more complex), the SQLS has a major advantage in resource usage as compared to VQLS.

system (L) and the number of qubits (n). However, a drawback of the SQLS that is directly inherited from the classical shadows approach is the exponential scaling in the locality of the Pauli strings, k , which is the reason behind our initial low-locality assumption (see Sec. III). A graphical representation of the scaling of $N_{circuits}/step$ as a function of L is reported for both algorithms in Fig. 2b. These results are obtained by assuming to have $n = 50$ qubits, corresponding to a $2^{50} \times 2^{50}$ linear system dimension, and a variable number of Pauli strings, $L \in [4, 2500]$, with locality $k \in [2, 3, 5, 7]$ for the SQLS case. The choice for the L domain is motivated by the assumption that it scales polynomially with n (i.e., we assumed $L_{max} = n^2 = 2500$). To ensure the same error in both procedures, we set $\epsilon_{hadamard} = \epsilon_{shadow} = 0.01$ for all the points, i.e., for the VQLS we took $n_{shots} = 10,000$. The plot in Fig. 2b demonstrates the exponential advantage of the SQLS as compared to the VQLS in terms $N_{circuits}/step$, for limited locality of the Pauli strings. We also stress that the pre-processing technique described in App. D can be used to simplify the linear system. In fact, it reduces the number and locality of the expectation values to evaluate the cost function. Anyway, this does not change the favourable scaling of the SQLS. The full investigation of the $N_{circuits}/step$ with pre-processing can be found in App. E.

B. Convergence time

In the second heuristic study we investigate the convergence times of the SQLS. In particular, we compare this char-

acteristic timescale to the corresponding one obtained in the VQLS. In the noiseless limit, the latter has been shown to provide a scaling as $\text{poly log}(N)\kappa \log(1/\epsilon)$. The convergence study was carried out with both methods for 4 different systems of equations, as follows.

First, we considered a 16×16 QLSP inspired by the Ising model [67] (IQLSP), described by the following operations

$$A_{IQLP} = \frac{1}{\zeta} \left(\sum_{i=1}^n \sigma_j^x + J \sum_{i=1}^{n-1} \sigma_j^z \sigma_{j+1}^z + \eta \sigma^I \right) \quad (21)$$

$$b_{IQLP} = H^{\otimes n} |0\rangle .$$

Then we considered two 16×16 randomly generated QLSP (also named RQLSP), as summarized by these operations

$$A_{RQLP} = \frac{1}{\zeta} \left(\sum_{i=1}^L c_i P_i^k + \eta \sigma^I \right) \quad (22)$$

$$b_{RQLP} = H^{\otimes n} |0\rangle .$$

Finally, we considered a 16×16 linear system derived from the discretized Laplace equation on a 2D grid, i.e., a Potential Grid Linear System (PGLS), as given by the following operations

$$A_{i,j} = \begin{cases} 0.22941573, & \text{if } i = j \\ -0.05735393, & \text{if } |i - j| = 1 \text{ or } |i - j| = 4 \\ 0, & \text{Otherwise} \end{cases} \quad (23)$$

$$b = \begin{cases} 0.5, & \text{if } i \leq 4 \\ 0, & \text{Otherwise} \end{cases} . \quad (24)$$

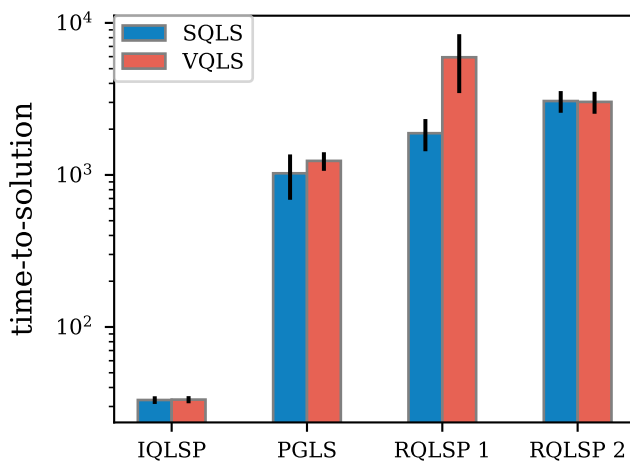


FIG. 3: A comparison of the time-to-solution for a number of different linear systems as obtained numerically by applying either the SQLS or the VQLS, respectively. By time-to-solution we mean the number of cost function evaluations required to guarantee a solution with precision ϵ (see Eq. (13)). For the Ising Inspired QLSP (IQLSP) we set the target $\epsilon = 0.01$, for the 16×16 Potential Grid Linear System (PGLS), we set the target $\epsilon = 0.02$, whilst for the randomly generated QLSP (RQLSP), we set $\epsilon = 0.1$ and $\epsilon = 0.05$, respectively. For all linear systems of equations considered, the two algorithms had equivalent errors, i.e., $\epsilon_{\text{hadamard}} = \epsilon_{\text{shadow}} = 0.01$ (i.e., for the VQLS this is equivalent to $n_{\text{shots}} = 10,000$). The heuristics have shown the SQLS to have a slightly favorable convergence time versus the VQLS, for an equal error, which cements the SQLS, alongside the results from Fig. 2, as a more resource-efficient algorithm to the solution of the QLSP. In addition, these results show that the SQLS has a poly logarithmic convergence in the system size N , in the noiseless limit.

Full details on these linear systems can be found in App. F.

The numerical experiments start with the creation of the linear systems of equations. The IQLSP is created with $J = 0.1$, and adjusting η and ζ such that the condition number is $\kappa = 60$ (see App. F for the explicit values). For the RQLSP, the locality of the matrices is set to $k = 2$, and η and ζ are adjusted such that the condition number for the matrix is $\kappa = 10$ in order to have manageable convergence times. Following these settings, all the examples are subjected to the classical pre-processing procedure, described in App. D, which reduces the complexity and quantity of expectation values to be calculated and, therefore, reduces the computational times of the simulations.

Then, a problem-specific ansatz is chosen for the different linear systems of equations. In the case of the IQLSP and the PGLS a real amplitude ansatz is used, whilst for the RQLSP a hardware efficient ansatz is used. For all systems, 4 layers of the respective ansatz are used during the optimization process. Full details on the parametrized circuit designs can be found in App. G. The numerical experiments consisted in solving

each linear system of equations with either the SQLS or the VQLS. In order to investigate the times-to-solution presented here in a consistent way, all systems are solved multiple times with different small parameter initializations [52–54]. Specifically, the IQLSP and the PGLS are solved 10 times, whilst the RQLSP1 and RQLSP2 are solved 5 times since they are more computationally intensive. In addition, for all experiments $\epsilon_{\text{hadamard}} = \epsilon_{\text{shadow}}$ as specified in the caption to Fig. 3. For the SQLS, the constant of proportionality related to Eq. (7) is set to 1.

Following the work in Ref. [68], we choose the numerical optimizers to be the modified Powell method [69] and Adam [70], which are shown to have similar convergence times. These optimizers are implemented through the Python Scipy library (Powell) [71], and the the Pennylane library (Adam optimizer) [59]. Due to the simplicity of the IQLSP, which guarantees smaller convergence times, the Powell optimizer is used for this system, whilst the PGLS, RQLSP1 and RQLSP2 use the Adam optimizer, since it guarantees slightly better convergence times. When the Adam optimizer is used, it is initiated with a learning rate of 0.1, which adaptively decreased to 0.001 during the optimization process. The latter is terminated when the trace distance (see Eq. (13)) reaches a threshold value. For the IQLSP the threshold trace distance is set to $\epsilon = 0.01$, for the PGLS the threshold trace distance is set to $\epsilon = 0.02$, while for RQLSP1 it is $\epsilon = 0.1$, and for the RQLSP2 we set $\epsilon = 0.05$.

A summary of the results obtained from these numerical experiments can be seen in Fig. 3. For all the systems we see that, for equal error, the SQLS has an advantageous/comparable convergence time when compared to the VQLS. We point out that this outcome is particularly relevant and noteworthy for two reasons. First, it guarantees the SQLS better overall resource usage as compared to the VQLS. In fact, given the arguments laid out in Sec. IV A, if the SQLS takes less/comparable time to converge and uses fewer resources per optimization step (in terms of the number of qubits, circuit depth and total N_{circuits} at equal error), then it has a better resource usage overall. Second, we claim that the convergence of the SQLS in the noiseless limit is upper bound by $\mathcal{O}(\text{polylog}(N)\kappa \log(1/\epsilon))$, which is the convergence of the noiseless VQLS. This guarantees the SQLS a poly-logarithmic scaling in the system size, which is an exponential advantage when compared to the best classical algorithm, and makes it a difficult problem to simulate classically.

C. Electrostatic Potentials in a Grid

As an example of practical application of the SQLS to a problem of physical nature, we show the results of the solution of a linear system derived from the discretization of the classical Laplace equation, i.e., $\nabla^2 \phi = 0$, on a two-dimensional (square) grid. We present this use case since it represents a linear system derived from the Laplace matrix [72], i.e., an object that commonly appears in various fields, such as ran-

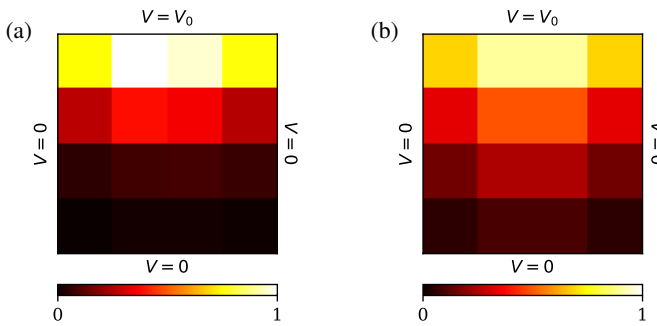


FIG. 4: The potentials derived from the solution of a 16×16 discretized Laplace equation onto a 4×4 2D grid. In (a) we show the solution that was reached using the SQLS, whilst in (b) we show the exact analytic solution. The solution reached with the SQLS has a 0.98 fidelity with the analytic one. Both solutions have been normalized to have the same color range and be directly comparable.

dom walks and analysis of electrical networks [73].

Essentially, the system we will be looking at is a $\sqrt{N} \times \sqrt{N}$ grid of potentials with a constant potential V_0 on the top boundary, and a null potential on all other boundaries. In this case the potentials inside the grid, $\vec{\phi}$, will be given by the linear system $A\vec{\phi} = \vec{b}$, where A is a $N \times N$ matrix, i.e., Eq. (25), and \vec{b} is a vector of size N , i.e., Eq. (26).

$$A_{i,j} = \begin{cases} 4, & \text{if } i = j \\ -1, & \text{if } |i - j| = 1 \text{ or } |i - j| = \sqrt{N} \\ 0, & \text{Otherwise} \end{cases} \quad (25)$$

$$\vec{b} = \begin{cases} V_0, & \text{if } i \leq \sqrt{N} \\ 0, & \text{Otherwise} \end{cases} \quad (26)$$

For the numerical experiments presented here, we take $N = 16$, which corresponds to the use of $n = \log(16) = 4$ qubits on a quantum register. In order to satisfy the norm condition on the matrix A , i.e., $\|A\|_2 \leq 1$, the matrix has to be normalized such that the values on the diagonal are equal to 0.22941573, and the off-diagonal values were equal to -0.05735393 . This left the choice of $V_0 = 0.5 \times \|A\|_2$ such that the normalization condition of \vec{b} is fulfilled after the normalization of the linear system. Thus the implementation on a quantum computer can be done using the unitary operation $U = \sigma^{J \otimes 2} \otimes H^{\otimes 2}$.

With this linear system at hand, the matrix A is decomposed into a linear combination of 4 unitaries using the theorem presented in Ref. [74]. More details on this algebraic result are given in App. H, for completeness. Since the matrix A is sparse, also the decomposed matrices will be sparse. Therefore, further decomposition can be achieved by implementing the algorithm developed by Ref. [61] to decompose each unitary as a linear sum of Pauli strings. The combination of these two procedures allows us to transform the full matrix A of Eq. (25) into a form that is suitable for the SQLS implementation. We also notice that other algorithms exist, which allow

to decompose a matrix A into linear sums of Pauli strings [57–61]. The system is then pre-processed by using the procedure described in App. D. The parameters are initialized to small values, which helps the optimization process [52–54]. The Adam optimizer [70] is chosen for the classical optimization steps, where the starting learning rate is set to 0.1, and it is adaptively decreased to 0.001 during the optimization process. For the optimization process, $\epsilon_{\text{shadow}} = 0.1$ for the first 250 iterations, which was then reduced to $\epsilon_{\text{shadow}} = 0.01$ for the rest of the optimization runs. This technique allows for the initial coarse-grained minimization of the cost function through a reduced number of resources, and then a fine-tuning using a larger number of resources only for the final part of the optimization process. This optimization has finally produced an approximate solution with 0.98 fidelity with the exact analytic solution of the same problem. The results are explicitly shown on the 4×4 grid in Fig. 4. In particular, the potential distribution of the approximate solution from the SQLS, shown in Fig. 4a, is compared to the exact solution of the same linear system of equations, represented on the same grid in Fig. 4b. We stress that the SQLS was able to produce a solution to a high precision, which is a good motivation that it might become a valid approach in solving real world linear systems of practical usefulness.

V. DISCUSSION

We have presented the Shadow Quantum Linear Solver (SQLS), a resource-efficient quantum algorithm to find the solution to the Quantum Linear System Problem (QLSP). By building upon recent work on variational algorithms to solve linear systems [36], and the resource-efficient framework of classical shadows [45], the SQLS appears to be the most promising variational algorithm to solve real systems of equations on NISQ hardware due to its convenience in resource usage, convergence times, and resilience to noise.

In particular, we have presented a series of analytic and heuristic studies that quantify various aspects of the SQLS. First, we find that the SQLS has better usage of the number of qubits, circuit depth, and number of circuits per cost function evaluation, when compared to the approach already present in the literature [36], which is the most resource-efficient variational algorithm to the QLSP known so far for limited locality, in all the three categories mentioned above. Furthermore, we have shown that the convergence times between the two algorithms, for an equal error, is more favorable for the SQLS. This is an indication that, in the noiseless limit, the SQLS has a scaling that goes as $\mathcal{O}(\text{poly log}(N) \kappa \log(1/\epsilon))$, in addition to an exponential advantage when compared to the best classical algorithms to solve large linear systems of equations. More than that, the resilience to global depolarization noise offered by the SQLS makes it an ideal candidate for current NISQ hardware. Finally, we were able to leverage techniques from linear algebra to apply the SQLS to a real physics problem, the discretized Laplace equation on a 2D grid. We also notice that the SQLS has room for significant improvement. On the side of classical shadows, further improve-

ments would include the implementation of a number of recent works that show how classical shadows can be optimized for the approximation of sums of expectation values of Pauli strings. Some of these techniques include the randomization schemes [75, 76], using locally biased classical shadows [77], principal eigenstate shadows [78], and dual frame optimization methods [79]. These techniques could either reduce the convergence times, for constant circuit executions, or diminish the number of executed circuits, for constant error. On side of Variational Quantum Algorithms side, in this work we have applied warm starting to the optimization process to solve the discretized 2D Laplace equation. Further studies may investigate this technique more in depth [46]. Other improvements include the possibility to use a dynamic ansatz [80]. An improved SQLS would then be subjected to a heuristic study to investigate the dependence of the convergence time on: the condition number κ , the error ε , and the system size N .

In summary, we believe that the method presented here could accelerate the development of practical solutions to the QLSP on NISQ devices. Furthermore, the paper highlights methods for converting complex linear systems into QLSPs, potentially inspiring novel approaches for solving systems of

linear equations using quantum computers.

ACKNOWLEDGMENTS

The authors acknowledge useful scientific discussions with A. Abbas, D. Cugini, S. El-Shawa, C. Macchiavello, D. Monaco, A. R. Morgillo, D. Nigro, G. Pellegrini, P. Perinotti, S. Roncallo, F. Tacchino, and S. Zanotti. F. Ghisoni would also like to acknowledge the use of high-performance computing cluster EOS at the Department of Mathematics, University of Pavia. D. Bajoni and D. Gerace acknowledge partial support from the ‘National Centre For HPC, Big Data and Quantum Computing’ (CN1, Spoke 10) within the Italian ‘Piano Nazionale di Ripresa e Resilienza (PNRR)’, Mission 4 Component 2 Investment 1.4 funded by the European Union - NextGenerationEU - project CN00000013. F. Scala and F. Ghisoni were supported by the ‘National Quantum Science Technology Institute’ (NQSTI, PE4, Spoke 1) within the PNRR project PE0000023.

[1] P. Wang, S. Mou, J. Lian, and W. Ren, Solving a system of linear equations: From centralized to distributed algorithms, *Annual Reviews in Control* **47**, 306 (2019).

[2] J. Rahola, Solution of dense systems of linear equations in the discrete-dipole approximation, *SIAM Journal on Scientific Computing* **17**, 78 (1996), <https://doi.org/10.1137/0917007>.

[3] B. Carpentieri, I. Duff, L. Giraud, and M. Magolu Monga Made, Sparse symmetric preconditioners for dense linear systems in electromagnetism, *Numerical Linear Algebra with Applications* **11**, 753 – 771 (2004), cited by: 32; All Open Access, Green Open Access.

[4] A. Frank, D. Fabregat-Traver, and P. Bientinesi, Large-scale linear regression: Development of high-performance routines, *Applied Mathematics and Computation* **275**, 411 (2016).

[5] R. P. Feynman, There’s plenty of room at the bottom (1959).

[6] M. A. Nielsen and I. L. Chuang, *Quantum Computation and Quantum Information* (Cambridge University Press, 2000).

[7] P. W. Shor, Polynomial-time algorithms for prime factorization and discrete logarithms on a quantum computer, *SIAM Journal on Computing* **26**, 1484–1509 (1997).

[8] L. K. Grover, A fast quantum mechanical algorithm for database search (1996), [arXiv:quant-ph/9605043 \[quant-ph\]](https://arxiv.org/abs/quant-ph/9605043).

[9] A. W. Harrow, A. Hassidim, and S. Lloyd, Quantum algorithm for linear systems of equations, *Physical Review Letters* **103**, 10.1103/physrevlett.103.150502 (2009).

[10] A. Ambainis, Variable time amplitude amplification and a faster quantum algorithm for solving systems of linear equations (2010), [arXiv:1010.4458 \[quant-ph\]](https://arxiv.org/abs/1010.4458).

[11] Y. Subaşı, R. D. Somma, and D. Orsucci, Quantum algorithms for systems of linear equations inspired by adiabatic quantum computing, *Physical Review Letters* **122**, 10.1103/physrevlett.122.060504 (2019).

[12] S. Chakraborty, A. Gilyén, and S. Jeffery, The power of block-encoded matrix powers: Improved regression techniques via faster hamiltonian simulation (Schloss Dagstuhl – Leibniz-Zentrum für Informatik, 2019).

[13] A. M. Childs, R. Kothari, and R. D. Somma, Quantum algorithm for systems of linear equations with exponentially improved dependence on precision, *SIAM Journal on Computing* **46**, 1920–1950 (2017).

[14] L. Wossnig, Z. Zhao, and A. Prakash, Quantum linear system algorithm for dense matrices, *Physical Review Letters* **120**, 10.1103/physrevlett.120.050502 (2018).

[15] N. Wiebe, D. Braun, and S. Lloyd, Quantum algorithm for data fitting, *Physical Review Letters* **109**, 10.1103/physrevlett.109.050505 (2012).

[16] B. D. Clader, B. C. Jacobs, and C. R. Sprouse, Preconditioned quantum linear system algorithm, *Physical Review Letters* **110**, 10.1103/physrevlett.110.250504 (2013).

[17] G. Wang, Efficient quantum algorithms for analyzing large sparse electrical networks (2017), [arXiv:1311.1851 \[quant-ph\]](https://arxiv.org/abs/1311.1851).

[18] P. Rebentrost, M. Mohseni, and S. Lloyd, Quantum support vector machine for big data classification, *Physical Review Letters* **113**, 10.1103/physrevlett.113.130503 (2014).

[19] I. Kerenidis and A. Prakash, Quantum recommendation systems (2016), [arXiv:1603.08675 \[quant-ph\]](https://arxiv.org/abs/1603.08675).

[20] J. Preskill, Quantum computing in the nisq era and beyond, *Quantum* **2**, 79 (2018).

[21] J. Wen, X. Kong, S. Wei, B. Wang, T. Xin, and G. Long, Experimental realization of quantum algorithms for a linear system inspired by adiabatic quantum computing, *Physical Review A* **99**, 10.1103/physreva.99.012320 (2019).

[22] M. AbuGhanem and H. Eleuch, Two-qubit entangling gates for superconducting quantum computers, *Results in Physics* **56**, 107236 (2024).

[23] S. A. Moses, C. H. Baldwin, M. S. Allman, R. Ancona, L. Ascarrunz, C. Barnes, J. Bartolotta, B. Bjork, P. Blanchard, M. Bohn, J. G. Bohnet, N. C. Brown, N. Q. Burdick, W. C. Burton, S. L. Campbell, J. P. Campora, C. Carron, J. Chambers, J. W. Chan, Y. H. Chen, A. Chernoguzov, E. Chertkov, J. Col-

ina, J. P. Curtis, R. Daniel, M. DeCross, D. Deen, C. Delaney, J. M. Dreiling, C. T. Ertsgaard, J. Esposito, B. Estey, M. Fabrikant, C. Figgatt, C. Foltz, M. Foss-Feig, D. Francois, J. P. Gaebler, T. M. Gatterman, C. N. Gilbreth, J. Giles, E. Glynn, A. Hall, A. M. Hankin, A. Hansen, D. Hayes, B. Higashi, I. M. Hoffman, B. Horning, J. J. Hout, R. Jacobs, J. Johansen, L. Jones, J. Karcz, T. Klein, P. Lauria, P. Lee, D. Liefer, S. T. Lu, D. Lucchetti, C. Lytle, A. Malm, M. Matheny, B. Mathewson, K. Mayer, D. B. Miller, M. Mills, B. Neyenhuis, L. Nugent, S. Olson, J. Parks, G. N. Price, Z. Price, M. Pugh, A. Ransford, A. P. Reed, C. Roman, M. Rowe, C. Ryan-Anderson, S. Sanders, J. Sedlacek, P. Shevchuk, P. Siegfried, T. Skripka, B. Spaun, R. T. Sprenkle, R. P. Stutz, M. Swallows, R. I. Tobey, A. Tran, T. Tran, E. Vogt, C. Volin, J. Walker, A. M. Zolot, and J. M. Pino, A race-track trapped-ion quantum processor, *Phys. Rev. X* **13**, 041052 (2023).

[24] Y. Kim, A. Eddins, S. Anand, K. X. Wei, E. van den Berg, S. Rosenblatt, H. Nayfeh, Y. Wu, M. Zaletel, K. Temme, and A. Kandala, Evidence for the utility of quantum computing before fault tolerance, *Nature* **618**, 500 (2023).

[25] M. Cerezo, A. Arrasmith, R. Babbush, S. C. Benjamin, S. Endo, K. Fujii, J. R. McClean, K. Mitarai, X. Yuan, L. Cincio, and P. J. Coles, Variational quantum algorithms, *Nature Reviews Physics* **3**, 625–644 (2021).

[26] M. Benedetti, E. Lloyd, S. Sack, and M. Fiorentini, Parameterized quantum circuits as machine learning models, *Quantum Science and Technology* **4**, 043001 (2019).

[27] J. Jäger and R. V. Krems, Universal expressiveness of variational quantum classifiers and quantum kernels for support vector machines, *Nature Communications* **14**, 10.1038/s41467-023-36144-5 (2023).

[28] A. Peruzzo, J. McClean, P. Shadbolt, M.-H. Yung, X.-Q. Zhou, P. J. Love, A. Aspuru-Guzik, and J. L. O’Brien, A variational eigenvalue solver on a photonic quantum processor, *Nature Communications* **5**, 10.1038/ncomms5213 (2014).

[29] Y. Cao, J. Romero, J. P. Olson, M. Degroote, P. D. Johnson, M. Kieferová, I. D. Kivlichan, T. Menke, B. Peropadre, N. P. D. Sawaya, S. Sim, L. Veis, and A. Aspuru-Guzik, Quantum chemistry in the age of quantum computing, *Chemical Reviews* **119**, 10856–10915 (2019).

[30] O. Higgott, D. Wang, and S. Brierley, Variational quantum computation of excited states, *Quantum* **3**, 156 (2019).

[31] T. Jones, S. Endo, S. McArdle, X. Yuan, and S. C. Benjamin, Variational quantum algorithms for discovering hamiltonian spectra, *Physical Review A* **99**, 10.1103/physreva.99.062304 (2019).

[32] F. Scala, S. Mangini, C. Macchiavello, D. Bajoni, and D. Gerace, Quantum variational learning for entanglement witnessing, in *2022 International Joint Conference on Neural Networks (IJCNN)* (IEEE, 2022).

[33] M. Lubasch, J. Joo, P. Moinier, M. Kiffner, and D. Jaksch, Variational quantum algorithms for nonlinear problems, *Physical Review A* **101**, 10.1103/physreva.101.010301 (2020).

[34] A. J. Pool, A. D. Somoza, C. M. Keever, M. Lubasch, and B. Horstmann, *Nonlinear dynamics as a ground-state solution on quantum computers* (2024), arXiv:2403.16791 [quant-ph].

[35] A. Pellow-Jarman, I. Sinayskiy, A. Pillay, and F. Petruccione, Near term algorithms for linear systems of equations, *Quantum Information Processing* **22**, 258 (2023).

[36] C. Bravo-Prieto, R. LaRose, M. Cerezo, Y. Subasi, L. Cincio, and P. J. Coles, Variational quantum linear solver, *Quantum* **7**, 1188 (2023).

[37] H.-L. Liu, Y.-S. Wu, L.-C. Wan, S.-J. Pan, S.-J. Qin, F. Gao, and Q.-Y. Wen, Variational quantum algorithm for the poisson equation, *Physical Review A* **104**, 10.1103/physreva.104.022418 (2021).

[38] Y. Liu, Z. Chen, C. Shu, P. Rebentrost, Y. Liu, S. Chew, B. Khoo, and Y. Cui, A variational quantum algorithm-based numerical method for solving potential and stokes flows, *Ocean Engineering* **292**, 116494 (2024).

[39] Y. Y. Liu, Z. Chen, C. Shu, S. C. Chew, B. C. Khoo, X. Zhao, and Y. D. Cui, Application of a variational hybrid quantum-classical algorithm to heat conduction equation and analysis of time complexity, *Physics of Fluids* **34**, 10.1063/5.0121778 (2022).

[40] H. Luo, Q. Zhou, Z. Li, and Y. Deng, Variational quantum linear solver-based combination rules in dempster–shafer theory, *Information Fusion* **102**, 102070 (2024).

[41] X. Xing, A. G. Cadavid, A. F. Izmaylov, and T. V. Tscherbul, *A hybrid quantum-classical algorithm for multichannel quantum scattering of atoms and molecules* (2023), arXiv:2304.06089 [quant-ph].

[42] C. J. Trahan, M. Loveland, N. Davis, and E. Ellison, A variational quantum linear solver application to discrete finite-element methods, *Entropy* **25**, 10.3390/e25040580 (2023).

[43] G. M. D’Ariano and P. Perinotti, Optimal data processing for quantum measurements, *Physical Review Letters* **98**, 10.1103/physrevlett.98.020403 (2007).

[44] S. Aaronson, Shadow tomography of quantum states (2018), arXiv:1711.01053 [quant-ph].

[45] H.-Y. Huang, R. Kueng, and J. Preskill, Predicting many properties of a quantum system from very few measurements, *Nature Physics* **16**, 1050–1057 (2020).

[46] F. Truger, J. Barzen, F. Leymann, and J. Obst, Warm-starting the vqe with approximate complex amplitude encoding (2024), arXiv:2402.17378.

[47] A. Basheer, Y. Feng, C. Ferrie, and S. Li, Alternating layered variational quantum circuits can be classically optimized efficiently using classical shadows (2022), arXiv:2208.11623.

[48] S. H. Sack, R. A. Medina, A. A. Michailidis, R. Kueng, and M. Serbyn, Avoiding barren plateaus using classical shadows, *PRX Quantum* **3**, 020365 (2022).

[49] J. R. McClean, S. Boixo, V. N. Smelyanskiy, R. Babbush, and H. Neven, Barren plateaus in quantum neural network training landscapes, *Nature Communications* **9**, 10.1038/s41467-018-07090-4 (2018).

[50] M. Larocca, S. Thanasilp, S. Wang, K. Sharma, J. Biamonte, P. J. Coles, L. Cincio, J. R. McClean, Z. Holmes, and M. Cerezo, *A review of barren plateaus in variational quantum computing* (2024), arXiv:2405.00781 [quant-ph].

[51] M. Cerezo, A. Sone, T. Volkoff, L. Cincio, and P. J. Coles, Cost function dependent barren plateaus in shallow parametrized quantum circuits, *Nature Communications* **12**, 10.1038/s41467-021-21728-w (2021).

[52] K. Zhang, L. Liu, M.-H. Hsieh, and D. Tao, *Escaping from the barren plateau via gaussian initializations in deep variational quantum circuits* (2022), arXiv:2203.09376 [quant-ph].

[53] C.-Y. Park and N. Killoran, Hamiltonian variational ansatz without barren plateaus, *Quantum* **8**, 1239 (2024).

[54] Y. Wang, B. Qi, C. Ferrie, and D. Dong, *Trainability enhancement of parameterized quantum circuits via reduced-domain parameter initialization* (2023), arXiv:2302.06858 [quant-ph].

[55] K. Sharma, S. Khatri, M. Cerezo, and P. J. Coles, Noise resilience of variational quantum compiling, *New Journal of Physics* **22**, 043006 (2020).

[56] A. Peruzzo, J. McClean, P. Shadbolt, M.-H. Yung, X.-Q. Zhou, P. J. Love, A. Aspuru-Guzik, and J. L. O’Brien, A variational eigenvalue solver on a photonic quantum processor, *Nature*

Communications **5**, [10.1038/ncomms5213](https://doi.org/10.1038/ncomms5213) (2014).

[57] R. M. N. Pesce and P. D. Stevenson, H2zixy: Pauli spin matrix decomposition of real symmetric matrices (2021), [arXiv:2111.00627 \[physics.comp-ph\]](https://arxiv.org/abs/2111.00627).

[58] S. Vidal Romero and J. Santos-Suárez, Paulicomposer: compute tensor products of pauli matrices efficiently, Quantum Information Processing **22**, [10.1007/s11128-023-04204-w](https://doi.org/10.1007/s11128-023-04204-w) (2023).

[59] V. Bergholm, J. Izaac, M. Schuld, C. Gogolin, S. Ahmed, V. Ajith, M. S. Alam, G. Alonso-Linaje, B. AkashNarayanan, A. Asadi, J. M. Arrazola, U. Azad, S. Banning, C. Blank, T. R. Bromley, B. A. Cordier, J. Ceroni, A. Delgado, O. D. Matteo, A. Dusko, T. Garg, D. Guala, A. Hayes, R. Hill, A. Ijaz, T. Isacsson, D. Ittah, S. Jahangiri, P. Jain, E. Jiang, A. Khandelwal, K. Kottmann, R. A. Lang, C. Lee, T. Loke, A. Lowe, K. McKiernan, J. J. Meyer, J. A. Montañez-Barrera, R. Moyard, Z. Niu, L. J. O’Riordan, S. Oud, A. Panigrahi, C.-Y. Park, D. Polatajko, N. Quesada, C. Roberts, N. Sá, I. Schoch, B. Shi, S. Shu, S. Sim, A. Singh, I. Strandberg, J. Soni, A. Száva, S. Thabet, R. A. Vargas-Hernández, T. Vincent, N. Vitucci, M. Weber, D. Wierichs, R. Wiersema, M. Willmann, V. Wong, S. Zhang, and N. Killoran, PennyLane: Automatic differentiation of hybrid quantum-classical computations (2022), [arXiv:1811.04968 \[quant-ph\]](https://arxiv.org/abs/1811.04968).

[60] T. Jones, Decomposing dense matrices into dense pauli tensors (2024), [arXiv:2401.16378 \[quant-ph\]](https://arxiv.org/abs/2401.16378).

[61] L. Hantzko, L. Binkowski, and S. Gupta, Tensorized pauli decomposition algorithm (2024), [arXiv:2310.13421 \[quant-ph\]](https://arxiv.org/abs/2310.13421).

[62] E. Knill and R. Laflamme, Power of one bit of quantum information, Physical Review Letters **81**, 5672–5675 (1998).

[63] T. Morimae, Hardness of classically sampling the one-clean-qubit model with constant total variation distance error, Physical Review A **96**, [10.1103/physreva.96.040302](https://doi.org/10.1103/physreva.96.040302) (2017).

[64] K. Fujii, H. Kobayashi, T. Morimae, H. Nishimura, S. Tamate, and S. Tani, Impossibility of classically simulating one-clean-qubit model with multiplicative error, Physical Review Letters **120**, [10.1103/physrevlett.120.200502](https://doi.org/10.1103/physrevlett.120.200502) (2018).

[65] A. Bernasconi, A. Berti, G. M. d. Corso, and A. Poggiali, Quantum subroutine for efficient matrix multiplication, IEEE Access **12**, 116274 (2024).

[66] V. Bergholm, J. Izaac, M. Schuld, C. Gogolin, S. Ahmed, V. Ajith, M. S. Alam, G. Alonso-Linaje, B. AkashNarayanan, A. Asadi, J. M. Arrazola, U. Azad, S. Banning, C. Blank, T. R. Bromley, B. A. Cordier, J. Ceroni, A. Delgado, O. D. Matteo, A. Dusko, T. Garg, D. Guala, A. Hayes, R. Hill, A. Ijaz, T. Isacsson, D. Ittah, S. Jahangiri, P. Jain, E. Jiang, A. Khandelwal, K. Kottmann, R. A. Lang, C. Lee, T. Loke, A. Lowe, K. McKiernan, J. J. Meyer, J. A. Montañez-Barrera, R. Moyard, Z. Niu, L. J. O’Riordan, S. Oud, A. Panigrahi, C.-Y. Park, D. Polatajko, N. Quesada, C. Roberts, N. Sá, I. Schoch, B. Shi, S. Shu, S. Sim, A. Singh, I. Strandberg, J. Soni, A. Száva, S. Thabet, R. A. Vargas-Hernández, T. Vincent, N. Vitucci, M. Weber, D. Wierichs, R. Wiersema, M. Willmann, V. Wong, S. Zhang, and N. Killoran, PennyLane: Automatic differentiation of hybrid quantum-classical computations (2022), [arXiv:1811.04968 \[quant-ph\]](https://arxiv.org/abs/1811.04968).

[67] F. Tacchino, A. Chiesa, S. Carretta, and D. Gerace, Quantum computers as universal quantum simulators: State-of-the-art and perspectives, Advanced Quantum Technologies **3**, [10.1002/qute.201900052](https://doi.org/10.1002/qute.201900052) (2019).

[68] A. Pellow-Jarman, I. Sinayskiy, A. Pillay, and F. Petruccione, A comparison of various classical optimizers for a variational quantum linear solver, Quantum Information Processing **20**, [10.1007/s11128-021-03140-x](https://doi.org/10.1007/s11128-021-03140-x) (2021).

[69] M. J. D. Powell, An efficient method for finding the minimum of a function of several variables without calculating derivatives, The Computer Journal **7**, 155 (1964), <https://academic.oup.com/comjnl/article-pdf/7/2/155/959784/070155.pdf>.

[70] D. P. Kingma and J. Ba, Adam: A method for stochastic optimization (2017), [arXiv:1412.6980 \[cs.LG\]](https://arxiv.org/abs/1412.6980).

[71] P. Virtanen, R. Gommers, T. E. Oliphant, M. Haberland, T. Reddy, D. Cournapeau, E. Burovski, P. Peterson, W. Weckesser, J. Bright, S. J. van der Walt, M. Brett, J. Wilson, K. J. Millman, N. Mayorov, A. R. J. Nelson, E. Jones, R. Kern, E. Larson, C. J. Carey, İ. Polat, Y. Feng, E. W. Moore, J. VanderPlas, D. Laxalde, J. Perktold, R. Cimrman, I. Henriksen, E. A. Quintero, C. R. Harris, A. M. Archibald, A. H. Ribeiro, F. Pedregosa, P. van Mulbregt, and SciPy 1.0 Contributors, SciPy 1.0: Fundamental Algorithms for Scientific Computing in Python, Nature Methods **17**, 261 (2020).

[72] . Chung, Fan R. K., *Spectral graph theory* (Providence, R.I. : American Mathematical Society, [1997] ©1997, [1997] "CBMS Conference on Recent Advances in Spectral Graph Theory held at California State University at Fresno, June 6-10, 1994"—T.p. verso.; Includes bibliographical references (pages 195-203) and index.

[73] P. G. Doyle and J. L. Snell, *Random walks and electric networks* (2000), [arXiv:math/0001057 \[math.PR\]](https://arxiv.org/abs/math/0001057).

[74] G. Pedersen, *Analysis Now*, Graduate texts in mathematics (Springer-Verlag, 1989).

[75] H.-Y. Huang, R. Kueng, and J. Preskill, Efficient estimation of pauli observables by derandomization, Physical Review Letters **127**, [10.1103/physrevlett.127.030503](https://doi.org/10.1103/physrevlett.127.030503) (2021).

[76] H.-Y. Huang, S. Chen, and J. Preskill, Learning to predict arbitrary quantum processes (2023), [arXiv:2210.14894 \[quant-ph\]](https://arxiv.org/abs/2210.14894).

[77] C. Hadfield, S. Bravyi, R. Raymond, and A. Mezzacapo, Measurements of quantum hamiltonians with locally-biased classical shadows (2020), [arXiv:2006.15788 \[quant-ph\]](https://arxiv.org/abs/2006.15788).

[78] D. Grier, H. Pashayan, and L. Schaeffer, Principal eigenstate classical shadows (2024), [arXiv:2405.13939 \[quant-ph\]](https://arxiv.org/abs/2405.13939).

[79] L. E. Fischer, T. Dao, I. Tavernelli, and F. Tacchino, Dual frame optimization for informationally complete quantum measurements (2024), [arXiv:2401.18071 \[quant-ph\]](https://arxiv.org/abs/2401.18071).

[80] H. Patil, Y. Wang, and P. S. Krstić, Variational quantum linear solver with a dynamic ansatz, Physical Review A **105**, [10.1103/physreva.105.012423](https://doi.org/10.1103/physreva.105.012423) (2022).

Appendix A: Optimal Parameter Resilience

In Ref. [36] it was proven that the cost function in Eq. (11) exhibits OPR to either global depolarization or measurement noise, respectively. Here we argue that the OPR to depolarization noise is maintained in the SQLS, whilst the OPR to measurement does not carry through.

The proof for OPR to global depolarization noise was based on 2 assumptions: the noise affects the estimation of the real and imaginary parts of all the terms in equal amounts, and the depth of the circuit is dominated by the ansatz. With regards to the first assumption, since the real and imaginary parts are calculated using the same shadows that are subjected to the same noise, then both would be equally affected. Concerning the second assumption, this is especially true in the SQLS, in which the circuit depth is wholly determined by the ansatz. Since the two assumptions on which the argument for OPR

to global depolarization noise for the VQLS hold also for the SQLS, it is possible to conclude that the SQLS has OPR to a global depolarization noise, simply following Ref. [36].

Regarding OPR to measurement noise, instead, we notice that it cannot be straightforwardly translated to the SQLS, and further studies are required to investigate its actual effects. First, we will assume that OPR to measurement noise in the context of the SQLS refers to OPR to the number of collected shadows. We believe this is a fair comparison since, just like with shots, the collection of shadows is what allows for the accuracy of the solution. We recall that the original proof of OPR to measurement noise is reliant on the modelling of each single-qubit measurement as a local depolarization channel. If the circuit measures only one qubit, which is the case for the Hadamard test, then the local depolarization channels can be modelled as a global depolarization channel. Since we already proved the OPR to a global depolarization channel, then the cost function also has OPR to measurement noise. The SQLS does not fit into this proof since the collection of the classical shadows requires the measurement of all qubits, and then the measurement noise cannot be modelled as a global depolarization noise, which allows to conclude that OPR to measurement noise (number of shadows) does not hold.

Appendix B: Hadamard test

Here we explain the details of the Hadamard test to calculate the terms β_{ij} and δ_{ijlp}^r of Eq. (15). The calculation of β_{ij} requires $n = \log_2(N)$ qubits, which are required to encode the state $V(\vec{\theta})|0\rangle^{\otimes n}$. An additional qubit is used as ancilla, initialized in the state $H|0\rangle = |+\rangle$, which is used to sequentially perform $C_a A_i^{k_i}$ and $C_a A_j^{k_j \dagger}$, where $C_a G$ represents the application of gate G on the main register controlled on the ancilla qubit. Finally, the application of a Hadamard gate followed by a measurement on the ancilla qubit is used to calculate the real part of β_{ij} . The estimation of the imaginary part of β_{ij} requires the ancilla to be initialized in the state $S^\dagger H|0\rangle$, instead, and then followed by the same operations. The circuit implementation can be seen in Fig. 2a(ii).

The calculation of δ_{ijlp}^r also requires $n = \log_2(N)$ qubits, which are needed to encode the state $V(\vec{\theta})|0\rangle^{\otimes n}$, as well as an additional ancillary qubit initialized in the state $|+\rangle$. Here, the operations to perform are: $C_a A_i^{k_i}$, $C_a U_l^{k_l \dagger}$, $C_a \sigma_r^z$, $C_a U_p^{k_p}$ and $C_a A_j^{k_j \dagger}$, where $C_a \sigma_r^z$ is a σ^z on the r^{th} qubit controlled on the ancilla. As before the imaginary part requires starting the ancilla qubit in the state $S^\dagger H|0\rangle$. This circuit is represented in Fig. 2a(iii). We notice that problem specific circuits can be devised to estimate the terms δ_{ijlp}^r and β_{ij} . These techniques typically double the number of qubits to reduce the number of large controlled operations to be performed.

Appendix C: Circuit count for the VQLS

Here we explain the details of the calculation of $N_{\text{circuits}}/\text{step}$ for the VQLS protocol, reported as a result in the main text, see Eq. (19). Due to the new form of the linear systems reported in Eq. (18), the calculation of the cost function requires to accurately estimate the terms $\delta_{ij}^r = \langle x|A_j^\dagger U \sigma_r^z U^\dagger A_i|x\rangle$ and $\beta_{ij} = \langle x|A_j^\dagger A_i|x\rangle$. We will start by considering the terms β_{ij} . By inspection, we see that if $i = j$ then $\beta_{ii} = 1$. Further inspection allows us to determine that $\beta_{ij} = (\beta_{ji})^*$, which, combined with the symmetry of the sum, implies that there is no need to calculate the imaginary part of the expectation values since they will all cancel out. This leaves $\frac{1}{2}L*(L-1)$ terms to approximate ω (Equation (17)).

As with regards to the term of the form of δ_{ij}^r , we notice that we can quarter the terms to be calculated since: $\delta_{ij}^k = (\delta_{ji}^k)^*$, and we are only interested in finding the real part of each expectation value. This leaves $\frac{n}{2} * L^2$ terms to find μ (Equation (16)). Using these considerations and assuming that each circuit is sampled with a constant number of shots n_{shots} , we finally find that the total number of quantum circuits that are needed to evaluate the cost function, including the shots, is given by

$$\frac{N_{\text{circuits}}}{\text{step}} = \frac{n_{\text{shots}}}{2} (L(L-1) + nL^2). \quad (\text{C1})$$

Appendix D: Pre-processing

Here we explain the details of the computationally cheap pre-processing technique that can be used to simplify linear systems of equations formulated as in Eqs. (9) and (10). The pre-processing performs the following steps: (i) it creates a list of all expectation values with associated coefficients that have to be calculated to evaluate the cost function; (ii) it then contracts all Pauli strings; (iii) it groups coefficients of all the contracted expectation values according to the terms in Eq. (15); (iv) it finally returns 2 lists, one containing the expectation values that have to be calculated for ω with the related coefficients, and one list for μ .

Given that the pre-processing operations will include at most scalar addition and Pauli string contractions, which are cheap since they are performed by using Pauli algebra, we can neglect the pre-processing time with respect to the total algorithmic time. The aim of this pre-processing procedure is to reduce the complexity and quantity of expectation values to be ultimately calculated in the SQLS.

Appendix E: Number of circuits per step with pre-processing

Here we present the heuristic study for $N_{\text{circuits}}/\text{step}$ calculated for the VQLS, VQLS with pre-processing, and the SQLS with pre-processing, respectively. In fact, the linear system of equations formalized in Eq. (18) can also be subjected to a computationally cheap classical algorithm, which simplifies

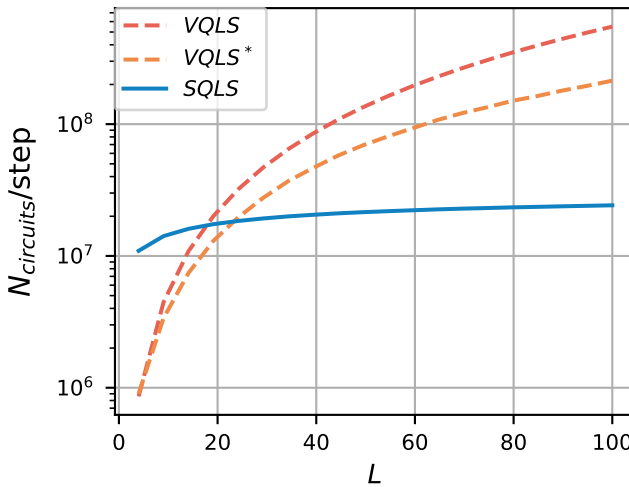


FIG. 5: Results for the quantity $N_{\text{circuits}}/\text{step}$ as a function of the number of terms in the linear system, L , for the different algorithms: VQLS, VQLS with pre-processing (VQLS*), and the SQLS (also with pre-processing). In this example, the numerical experiment created 30 random $2^{10} \times 2^{10}$ (i.e., 10 qubits dimensional space) linear problems with fixed number of Pauli strings, $L \in [4, 100]$, and fixed locality, $k = 2$, calculating $N_{\text{circuits}}/\text{step}$ for each procedure. The plot shows that even with pre-processing, the SQLS displays an exponential advantage with the scaling when compared to the VQLS.

number and complexity of the terms in the cost function, as shown in App. D. A pre-processed cost function can be evaluated using both the Hadamard test and classical shadows. By defining the number of terms to evaluate the cost function after the pre-processing as N_{PP} , the Hadamard test requires $N_{\text{PP}} \times n_{\text{shots}}$ circuit executions, and it will be referred to as VQLS*, whilst in classical shadows $N_{\text{circuits}}/\text{step}$ is determined by Eq. (7), in which we take $M = N_{\text{PP}}$; we will refer to this case as SQLS in the plots.

In our numerical experiment, this study required the creation of 30 random $2^{10} \times 2^{10}$ (10 qubit) linear problems with fixed number of Pauli strings, $L \in [4, 100]$, and fixed locality $k = 2$. These were then used to find $N_{\text{circuits}}/\text{step}$ for: the VQLS (Equation (19)), the VQLS with the pre-processing, $N_{\text{PP}} \times n_{\text{shots}}$, and the SQLS, where the number of operators was $M = N_{\text{PP}}$. The results for $N_{\text{circuits}}/\text{step}$ as a function of the number of terms in the linear system, L , is reported in Fig. 5. Overall, we see that the scaling of the number of circuits per optimization step remains favourable to the SQLS, also in the case of pre-processing in the VQLS, which shows a resource advantage for the SQLS in terms of $N_{\text{circuits}}/\text{step}$.

Appendix F: Linear Systems

Here we report further details about the linear system of equations that were used as part of the comparative investigation reported in Sec. IV B. The matrix A for the QLSP inspired

by the Ising model (IQLSP) is explicitly given by

$$A_{\text{IQLSP}} = 0.0123(ZZII - IZZI - IIIZ) + 0.123(XIII + IXII + IIXI + IIIX) + 0.508III \quad (\text{F1})$$

The corresponding matrices for the Random QLSP (RQLSP) are explicitly given by

$$A_{\text{RQLSP1}} = -0.0513IXXI - 0.366IIYY - 0.0352XXII + 0.144IXIZ + 0.55III \quad (\text{F2})$$

and

$$A_{\text{RQLSP2}} = 0.242ZZII - 0.0817IZZI + 0.183XIIX - 0.0780IZIY + 0.55III, \quad (\text{F3})$$

respectively.

Appendix G: Variational ansatz

Here we present the ansatzes that were used throughout the numerical experiments whose results are reported in Sec. IV B. For the two RQLSP's we used a hardware efficient ansatz of the form represented in Fig. 6a. Given that these systems were hardware efficient, and they could have involved real and complex elements, the choice of this ansatz was to keep the parameter search space as hardware efficient as possible. Therefore, all Pauli rotations (R_X, R_Y, R_Z) were used, and CNOTs in a ring structure were used to connect all the elements. When applied to a 4 qubits register, this ansatz requires 12 parameters per layer.

For the IQLSP and the potential grid, we used the real amplitude ansatz, which is reported in Fig. 6b. The motivation behind this choice was that for both of these linear systems, A and b were only composed of real elements, and therefore also the solution must have been composed of real elements. Therefore, the ansatz that was used was only composed of R_Y rotations and CNOTs.

Appendix H: Matrix Decomposition

Here we present a simplified version of the theorem reported in Ref. [74], which establishes the rule for the decomposition of a matrix into a linear sum of unitary matrices.

First, we notice that any complex matrix can be represented as:

$$A = B + iC, \quad (\text{H1})$$

in which

$$B = \frac{1}{2}(A + A^*) \quad (\text{H2})$$

$$C = \frac{1}{2i}(A - A^*). \quad (\text{H3})$$

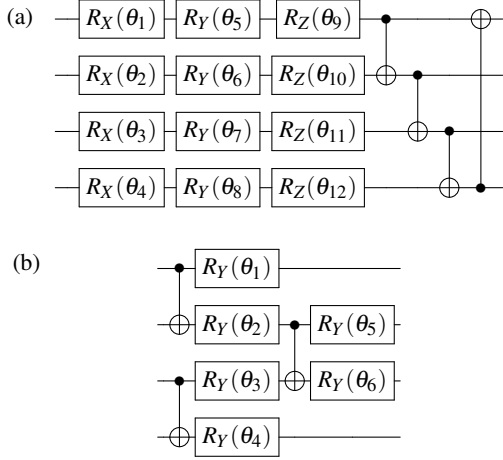


FIG. 6: (a) The hardware efficient ansatz that was used to find a solution to systems (F2) and (F3) and (b) the real amplitude ansatz that was used to find the solution to linear systems (F1) and (23)

If we assume that $\|A\|_2 \leq 1$, then $\|B\|_2 \leq 1$ and $\|C\|_2 \leq 1$ are

both true. Therefore, we can further decompose B as:

$$B = \frac{1}{2}(U_B + V_B) \quad (H4)$$

with

$$U_B = B + i\sqrt{I - B^2} \quad (H5)$$

$$V_B = B - i\sqrt{I - B^2}, \quad (H6)$$

and similarly

$$C = \frac{1}{2}(U_C + V_C), \quad (H7)$$

with

$$U_C = C + i\sqrt{I - C^2} \quad (H8)$$

$$V_C = C - i\sqrt{I - C^2}. \quad (H9)$$

By inspection, this breakdown can be seen to be true. Furthermore, we can see that $(U_B)^* = V_B$ and $(U_C)^* = V_C$. Finally $U_B V_B = V_B U_B = \mathbb{I}$, and $U_C V_C = V_C U_C = \mathbb{I}$. In the end, we have decomposed the matrix A into a linear combination of 4 unitary matrices of the form

$$A = \frac{1}{2}U_B + \frac{1}{2}V_B + \frac{i}{2}U_C + \frac{i}{2}V_C. \quad (H10)$$